

Highlights

Low latitude geomagnetic response associated with intense geomagnetic storms: regional space weather in Mexico

Castellanos-Velazco, C. I., Corona-Romero, P., González-Esparza, J. A., Sergeeva, M. A., Caccavari-Garza, A. L., Gatica-Acevedo, V. J.

- Research of space weather activity over center of Mexico
- Analysis of differences in local and planetary geomagnetic responses during a geomagnetic storm.
- Study of ionospheric currents related to geomagnetic storms, known to drive local geomagnetic fluctuations.

Low latitude geomagnetic response associated with intense geomagnetic storms: regional space weather in Mexico

Castellanos-Velazco, C. I.^a, Corona-Romero, P.^{b,c,d}, González-Esparza, J. A.^{c,d}, Sergeeva, M. A.^{b,c,d}, Caccavari-Garza, A. L.^d and Gatica-Acevedo, V. J.^{c,d,**}

^aPosgrado en Ciencias de la Tierra, Universidad Nacional Autónoma de México, Cto. de los Posgrados S/N, C.U., Ciudad de México, 04510, Ciudad de México, México.

^bInvestigadores por México-CONAHCYT (CONAHCYT Research Fellow), Instituto de Geofísica Unidad Michoacán, Universidad Nacional Autónoma de México, Morelia, Michoacán, México.

^cLaboratorio Nacional de Clima Espacial (LANCE), Instituto de Geofísica Unidad Michoacán, Universidad Nacional Autónoma de México, Antigua Carretera a Pátzcuaro 8701, Morelia, 58089, Michoacán, México.

^dInstituto de Geofísica, Universidad Nacional Autónoma de México, Av. Universidad 3000, México city, 04150, México.

ARTICLE INFO

Keywords:

Regional Space Weather
Regional Geomagnetic Response
Local Ionospheric Effects
Disturbed Dynamo Current
Disturbed Polar Current 2
Regional Geomagnetic Indices

ABSTRACT

In this work we studied the regional manifestations of space weather at central Mexico through isolate the local geomagnetic response from its planetary counterpart. In order to do so, we analyzed 20 intense geomagnetic storms by identifying the ionospheric contribution in their regional geomagnetic data as registered at the Magnetic Observatory of Teoloyucan (located at the north of Mexico City). Our analysis indicated that local geomagnetic response is mainly driven by ionospheric disturbances. We also found that the *disturbed polar current number 2* and the *disturbed dynamo current* are particularly relevant for the regional geomagnetic response. Additionally, we showed that regional geomagnetic activity can be approximated by the combined effects of the planetary geomagnetic response and the regional magnetic perturbations induced by the commented ionospheric currents. Finally, our results highlights the particularities that geomagnetic response has at regional scales.

1. Introduction

Geomagnetic storms (*GS*) are significant phenomena within space weather, as they can adversely impact various systems such as communications, navigation, and energy supply (Schrijver, 2015). *GSs* are closely tied to solar activity and primarily involve a temporary weakening of the Earth's magnetic field (*EMF*), among other effects (Gonzalez et al., 1994). These storms arise when solar wind material penetrates the *EMF* through magnetic reconnection between the interplanetary magnetic field (*IMF*) and the *EMF* (see Baumjohann and Treumann, 1999; C.T Russell, 2016, and references there in).

GS are typically identified using geomagnetic indices, which quantify their magnitude. Various geomagnetic indices exist, each designed to capture specific aspects of geomagnetic disturbances. In the context of middle and low latitudes, the most commonly used indices are the planetary K index (K_P) and the disturbance storm time index (Dst). These indices are especially effective in regions where the geomagnetic perturbation can be observed on the Earth's magnetic

field's horizontal component (H). The K_P index quantifies the maximum variation in H observed at mid-latitudes over three-hour intervals. Similarly, the Dst index represents an hourly average of perturbations in H as measured near the Earth's magnetic equator. These planetary indices, namely K_P and Dst , have regional counterparts that rely on regional data instead of planetary averages (Mayaud, 1980).

While *GSs* are global phenomena, their manifestation at the regional scale can exhibit variability across different locations. This variation can be attributed to the Earth's heterogeneity, asymmetries in magnetospheric and ionospheric currents, and the intricate interactions between the magnetosphere and ionosphere in each region. Consequently, geomagnetic latitude, local time, and seasonal variations can influence how a *GS* unfolds at the regional level. Overlooking these regional factors may lead to uncertainties and misinterpretations when attempting to comprehend and address the potential effects and risks of *GSs* (Pirjola, 2000; Bailey et al., 2017; Vodyannikov et al., 2006; da Silva Barbosa et al., 2015).

In recent decades, there has been growing interest in regional space weather. Regional space weather studies mainly focuses on identified the differences between the local and planetary geomagnetic and ionospheric responses (see Hejda and Bochníček, 2005; da Silva Barbosa et al., 2015; Bailey et al., 2017, and references there in). Because such differences, combined with a knowledge of the regional distribution of sensitive

*Corresponding author

 ccastellanos@igeofisica.unam.mx (C.C. I.);
p.coronaromero@igeofisica.unam.mx (C. P.);
americo@igeofisica.unam.mx (.G.J. A.)
ORCID(s): 0000-0001-8818-5318 (C.C. I.);
0000-0002-2573-2967 (C. P.); 0000-0003-4774-1829 (.G.J. A.)

infrastructure and facilities as well as services demand, might improve the management of risks due to space weather (Schrijver, 2015).

Recently, Mexico has joint this regional space weather studies by conduct scattered regional ionospheric and geomagnetic studies (*e.g.* Pérez-Enríquez and Kotsarenko, 2003; Gonzalez-Esparza et al., 2005; Rodriguez-Martinez et al., 2011; Carrillo-Vargas et al., 2012; Rodriguez-Martinez et al., 2011; López-Montes et al., 2012; Rodriguez-Martinez et al., 2014; Merline Matamba et al., 2016; Martínez-Bretón L. et al., 2016). However, the systematic study and monitoring of regional space weather formally commenced in 2014 with the initiation of operations by the Mexican Space Weather Service (SCIESMEX) at the Geophysics Institute (IGF) of the National Autonomous University of Mexico (UNAM). Subsequently, by 2016, a significant expansion of infrastructure and technologies dedicated to studying and monitoring regional space weather was achieved by establishing the Mexican Space Weather National Laboratory (LANCE) at IGF-UNAM (Gonzalez-Esparza et al., 2017).

Through collaborative efforts and resource sharing, the SCIESMEX/LANCE collaboration has identified the potential role of ionospheric disturbances in driving regional geomagnetic response during *GS* periods (see Romero-Hernandez et al., 2017; Sergeeva et al., 2017, 2019; Corona-Romero et al., 2018, 2017). This finding aligns with other studies conducted in mid and low latitudes, as it is known that for these latitudinal ranges, two primary sources of geomagnetic fluctuations driven by ionospheric currents exist: the *disturbed polar current number 2 (DP2)* (Nishida, 1968a,b, 1966), and the *disturbed dynamo current (Ddyn)* (Blanc and Richmond, 1980).

On one hand, the *DP2* current is linked to electric fields induced during the magnetic reconnection between the interplanetary magnetic field and the *EMF*. These electric fields are then transported along the Birkeland currents (Wei et al., 2015; Kikuchi and Hashimoto, 2016), eventually reaching high ionospheric latitudes where they give rise to a pattern of two ionospheric convective twin cells known as *DP2* currents. The charged particles within these cells are carried by the centrifugal and curvature effects of the *EMF*, resulting in the induction of a polarized electric field (Heppner, 1972b,a; Bobova et al., 1985; Blanc and Caudal, 1985; Denisenko et al., 1992). During the main phase of a *GS*, this polarized electric field, coupled with the *DP2* current, can extend beyond high latitudes, encompassing mid and even low latitudes (Nishida, 1966, 1968a; Obayashi and Nishida, 1968).

On the other hand, *Ddyn* currents represent amplifications of the polar ionospheric currents due to the precipitation of energetic particles during the main phase of a *GS*. The resulting Joule heating in the thermosphere generates the circulation of neutral winds

and charged particles in the equatorward direction. The Coriolis force induces a westward shift in the direction of these polar-equatorial flows at mid and low latitudes (Blanc and Richmond, 1980; Le Huy and Amory-Mazaudier, 2005; Zaka et al., 2009). Equatorward Pedersen currents are induced in this process, leading to the accumulation of charged particles along the dip equator. This accumulation, in turn, triggers the generation of poleward-directed electric fields and a second Pedersen current in the same direction but opposing the first one. Consequently, Hall currents are driven eastward at mid-latitudes (approximately 45°), and these currents are interrupted at termination points (Blanc and Richmond, 1980). This sequence of events results in currents diverging and closing at adjacent latitudes, forming the distinct vortex-shaped currents known as *Ddyn*.

Previous studies indicate that the effects associated with *Ddyn* and *DP2* locally disrupt the total electron content, causing significant impacts on services such as telecommunications and global positioning systems during periods of *GSs*, regardless of geomagnetic latitude (Yamazaki et al., 2016; Akala et al., 2020; Vankadara et al., 2022). In the case of Mexico, a local ionospheric response has been observed even when the Dst index is slightly perturbed (Sergeeva et al., 2017, 2019). Given that the *Ddyn* and *DP2* ionospheric currents possess the potential to influence the geomagnetic response in mid and low latitudes, it raises the question of whether these ionospheric mechanisms are responsible for linking regional geomagnetic response to local ionospheric perturbations in central Mexico. This inquiry constitutes the primary motivation for our study.

Throughout this work, we first seek to identify disparities between regional and planetary geomagnetic activities to isolate regional geomagnetic responses during *GSs*. With this regional response isolated, we search for evidence of *Ddyn* and *DP2* mechanisms as sources of such regional geomagnetic response. Our approach involves identifying their respective signatures within magnetic records. Subsequently, we validate our findings by comparing planetary and regional geomagnetic activity indices, culminating in a discussion of our concluding remarks. In the next section, we present the methodology employed to accomplish these objectives and provide further insights of our investigation.

2. Methodology

2.1. Local geomagnetic response

We analyzed 20 *GS* events to identify the regional geomagnetic response. These events occurred during the period from 2003 to 2018, encompassing the descending phase of solar cycle 23 and almost all of solar cycle 24. The data were recorded at the Geomagnetic Observatory of Teoloyucan (TEO),

Table 1

Study Cases. From left to right: event number, GS start date, minimum(maximum) values reached by Dst (K_p) and ΔH (K_{MEX}), respectively.

| Event # | Beginning of main phase | ^a Dst minimum [nT] | ^b ΔH minimum [nT] | ^a K_p maximum | ^b K_{MEX} maximum |
|---------|-------------------------|---------------------------------|--------------------------------------|----------------------------|--------------------------------|
| 1 | 2003/05/29 | -144 | -190 | 8+ | 9 |
| 2 | 2003/10/14 | -85 | -126 | 7+ | 7- |
| 3 | 2003/11/20 | -422 | -441 | 9- | 9 |
| 4 | 2004/07/22 | -170 | -167 | 9- | 8+ |
| 5 | 2004/08/30 | -129 | -154 | 7 | 7- |
| 6 | 2004/11/08 | -374 | -398 | 9- | 9 |
| 7 | 2005/05/15 | -247 | -206 | 8+ | 7 |
| 8 | 2005/06/12 | -106 | -120 | 7+ | 6+ |
| 9 | 2005/08/24 | -184 | -138 | 9- | 9- |
| 10 | 2005/08/31 | -122 | -125 | 7 | 6+ |
| 11 | 2006/08/19 | -79 | -131 | 6 | 7- |
| 12 | 2006/12/14 | -162 | -247 | 8+ | 9 |
| 13 | 2015/03/15 | -222 | -282 | 8 | 8- |
| 14 | 2015/10/07 | -124 | -143 | 7+ | 7+ |
| 15 | 2015/12/20 | -155 | -189 | 7- | 7 |
| 16 | 2016/03/06 | -98 | -120 | 6 | 7 |
| 17 | 2016/10/13 | -104 | -128 | 6+ | 6+ |
| 18 | 2017/05/27 | -125 | 145 | 7 | 8 |
| 19 | 2017/09/07 | -124 | -170 | 8+ | 8+ |
| 20 | 2018/09/25 | -175 | -176 | 7+ | 7- |

Comments for the Table.

^a Dst and K_p were obtained from the International Service of geomagnetic Indices (ISGI).

^b Regional geomagnetic indices ΔH and K_{MEX} were computed by the Space Weather National Laboratory, using TEO geomagnetic registers.

located at 27.84°N and 28.41°W. TEO is operated by the Magnetic Service of the Geophysics Institute at the National Autonomous University of Mexico. We selected events with a local K index (K_{MEX}) equal to or larger than 6+ and ΔH (the regional equivalent of the Dst index) below -120 nT. We also rejected events whose datasets contained a considerable amount of missing data. Table 1 provides details of all the analyzed events.

We assume that significant differences between regional and planetary geomagnetic indices should be provoked by local geomagnetic response. Thus, in order to identify such differences we directly compare Dst and ΔH for our studied events. Figure 1 shows a dispersion plot that compares the regional response (vertical axis) with its planetary counterpart (horizontal axis). In the figure we observe two well differentiated tendencies in data distribution: The first one ($Dst \geq -100$ nT) where the data points closely follow the identity (solid black line), and the second one (green shadowed region) where the data dispersion detached from the identity ($Dst < -100$ nT). These trends align with correlation indices, yielding $R^2 = 0.77$ for the former and $R^2 = 0.42$ for the latter.

Figure 1 shows, in the case of our analyzed events, that planetary and regional geomagnetic indices may significantly differ each other. Which in turn suggests the presence of some kind of local (ionospheric) mechanisms with the capability to deviate the regional value of geomagnetic field from its planetary counterpart. Hence, we need to identify in the regional geomagnetic registers the signatures for the magnetic contribution cause by those local mechanisms (Le Huy and Amory-Mazaudier, 2005; Zaka et al., 2009; Amory-Mazaudier et al., 2017; Younas et al., 2020). Now we proceed to identify such mechanisms.

2.2. Geomagnetic signatures of local ionospheric currents

The local values of EMF are result from the contribution of many sources (Rishbeth and Garriott, 1969; Knecht and B.M, 1985; Gjerloev, 2012; van de Kamp, 2013). In the particular case of the horizontal component (H) of local EMF , we can express it as:

$$H = B_{SQ} + H_0 + D_M + D_I. \quad (1)$$

With B_{SQ} is the diurnal variation obtained from the local quiet days (van de Kamp, 2013) and H_0 is the day-to-day variation (Gjerloev, 2012; van de Kamp, 2013).

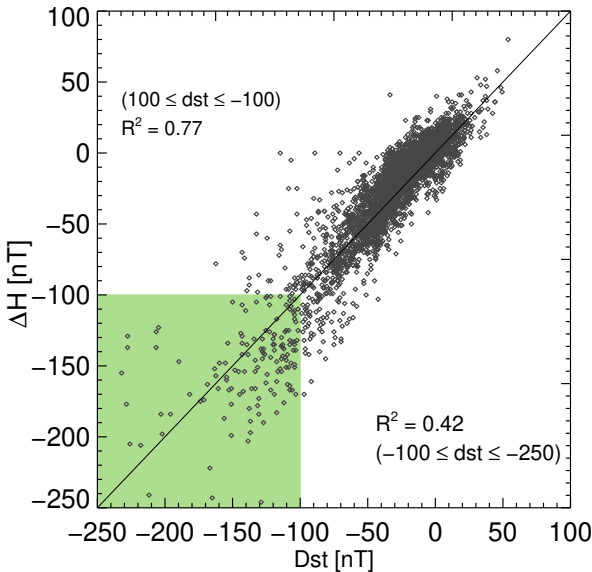


Figure 1: Dispersion plot of regional and planetary geomagnetic responses as registered by ΔH (vertical axis) and Dst (horizontal axis) for all analyzed events. The figure also shows the correlation indices for data with $Dst \geq -100$ nT and $-250 \leq Dst < -100$ nT (shadowed-green region).

The last two terms are irregular magnetic variations related to geomagnetic activity (Le Huy and Amory-Mazaudier, 2005; Zaka et al., 2009), with D_M being the contribution from (planetary scale) magnetospheric currents, and D_I is the magnetic contribution driven by ionospheric perturbations. In addition, since we are at mid and low latitudes, $D_M \approx Dst \cos(\lambda)$, with λ being the geomagnetic latitude (Amory-Mazaudier et al., 2017). Therefore, we can express D_I as:

$$D_I \approx H - (B_{SQ} + H_0 + Dst \cdot \cos(\lambda)). \quad (2)$$

Furthermore, we can also express D_I as:

$$D_I = DP2 + Ddyn + D_{others}, \quad (3)$$

Where D_{others} refers to ionospheric perturbations distinct from the disturbed polar current number 2 ($DP2$) and the disturbed dynamo current (D_{dyn}). These two ionospheric currents are well accepted sources for local geomagnetic fluctuations in low and mid geomagnetic latitudes, as discussed in the Introduction.

3. Analysis and results

3.1. Local ionospheric disturbances and induced magnetic fluctuations

In this section, we present our analysis process through showing the analysis of events 3, 6, 13 and 18. The panels (a) of Figure 2 show the profiles of Dst (black) and ΔH (green) indices during the storm period associated with events (see Table 1). In the panels we observe that both indices are *quiet* up to the start

of the GS's main phase, signed out by a (left-sided) vertical dotted line. The main phase provokes the values of Dst and ΔH indices to decrease up to reaching a minimum. Once this minimum value is reached, start the recovering phases where the magnetic indices slowly tend to recover their *quiet* (pre-storm) value. This phase regularly extends for several hours or even days up to the end of the GS (right-side vertical dotted line).

In the panels (b) of Figure 2, we appreciate the resulting profile of D_I (Equation (2)), which we computed using the ΔH and the Dst reported data. It is remarkable that all D_I profiles shown in Figure 2 significantly differ each other. Subsequently, we compute the power spectrum of each D_I , which we show in panels (d) of Figure 2. In the power spectra, we highlight, by a gray shading, the range of periods(frequencies) consistent with $DP2$ and $Ddyn$. It is important to comment that we manually identify $Ddyn$'s range by setting the main period and searching potency peaks within the range of possible harmonics. These slightly variations on periods(frequencies) are due to the differences between our study cases, already commented.

In panels (c) of Figure 2 we present the profiles of the induced magnetic perturbations caused by $DP2$ (solid red line) and $Ddyn$ (solid black line). These profiles are constructed departing from the frequencies identified through the filtering process commented on in the previous paragraph. We note that the enhancements of the induced effects of $Ddyn$ and $DP2$ simultaneously occur with significant variations in the total electron content (ΔTEC) over central Mexico, as the panels (e) of Figure 2 shows.

We applied the procedure described in this section to all our study cases. The Figures 6 and 7 in the Appendix A show the results from our analysis. In general, we noted that the amplitude of the magnetic oscillations induced by $Ddyn$ tend to be larger than those induced by $DP2$ (see Figures 6 and 7 at the Appendix A). This suggests that, in most cases, the intensity of $Ddyn$'s induced magnetic effects are larger than those induced by $DP2$, and thus $Ddyn$'s effects are also dominant on the local EMF.

We believe that the process that triggers the GS itself may affect the evolution of the ionospheric response, directly modifying the evolution of $DP2$ and $Ddyn$ currents. Secondly, we have to consider that our data is sampled in hourly resolution. In this case, data sampling represents an important limitation since $DP2$ magnetic fluctuations, as mentioned in Nishida (1968b), may have periods of less than an hour or even of tens of minutes. In this scenario, we possibly missed part of $DP2$ fluctuations and potency during our analysis. This could be solved, in principle, by using $Sym - H$ index rather than Dst , a task which exploration we consider as future work.

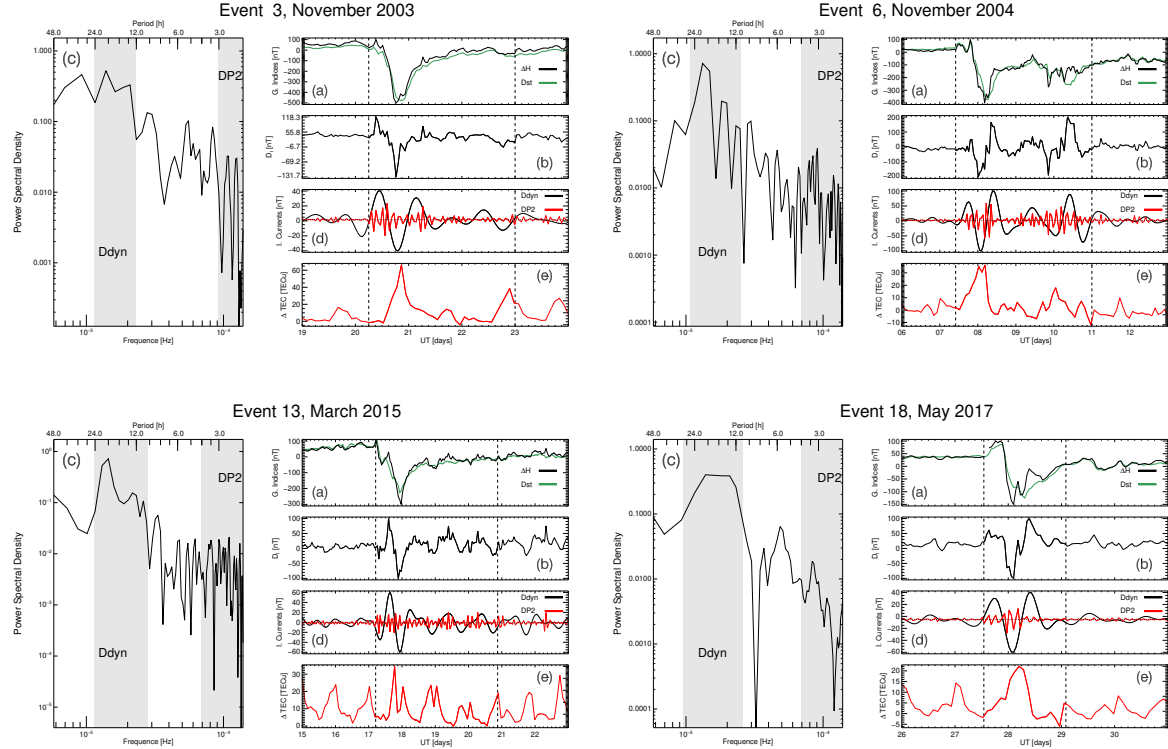


Figure 2: Analysis examples from solar cycle 23 (upper panels) and solar cycle 24 (bottom panels). Upper (bottom) panels show the analysis of events 3 (13) and 6 (18). The analysis of each event is made up of five different processes represented by panels labeled with letters. Panels (a) present the values of Dst (black line) and ΔH (green line) indices during the event. Panels (b) show the computed value of D_I . Panels (c) show the power spectrum associated to D_I . Panels (d) show the induced geomagnetic effects of $Ddyn$ (in black) and $DP2$ (in red) reconstructed from the filtered power spectrum. Panels (e) show the variation of the total electron content ($\Delta TEC = TEC - \langle TEC \rangle$) over the central region of Mexico. The dotted vertical lines in panels (a), (b), (d) and (e) mark out the start (left-sided) and end (right-sided) of the GS. Gray shaded regions in panel (c) highlight the bandwidths associated with $Ddyn$ and $DP2$.

3.2. Validation of DP2 and Ddyn magnetic signatures

In Section 2.1 we were able to identify significant differences between the planetary and regional geomagnetic activity. Condition that we associated to regional geomagnetic response. Subsequently, in Section 3.1, we identified the tentative geomagnetic mechanisms for that regional geomagnetic response. Such mechanism are the $Ddyn$ and $DP2$ ionospheric currents, whose effects were reconstructed by a periods (frequencies) filtering process. We also learned that those effects are systematically associated with local perturbations on TEC . Now, we require to validate our results.

In order to validate our previous results, first we approximate the regional geomagnetic index ΔH , which can be defined as:

$$\Delta H = H - (B_{SQ} + H_0), \quad (4)$$

through Dst and the resulting profiles of $DP2$ and $Ddyn$. Thus, by manipulating Equations (2), (3) and (4) we obtain that:

$$\Delta H \approx \cos(\lambda)Dst + DP2 + Ddyn. \quad (5)$$

For simplicity, we call Dst_λ the combined effects of $\cos(\lambda)Dst$, $DP2$ and $Ddyn$:

$$Dst_\lambda = \cos(\lambda)Dst + DP2 + Ddyn. \quad (6)$$

In our context, Dst_λ represents the combined effects of planetary geomagnetic response translated at the geomagnetic latitude (λ) of central Mexico and the regional geomagnetic effects of $DP2$ and $Ddyn$. Hence, our first step for validation is to corroborate that our computed value of Dst_λ approximates ΔH . In addition, we can also used Dst_λ and the values of K_p to approximate the local value of K .

The results of the validation process commented on before applied on events 3, 13 and & 18 are shown by Figure 3. The upper panels of Figure 3 compares the profiles of ΔH (black), Dst (green) and Dst_λ (red). In the panel we note that Dst_λ is systematically closer to ΔH than Dst . This condition holds during the main and recovering phases of the GS.

This process was repeated with all our study cases. The Figures 8 and 9 show the results of our validation

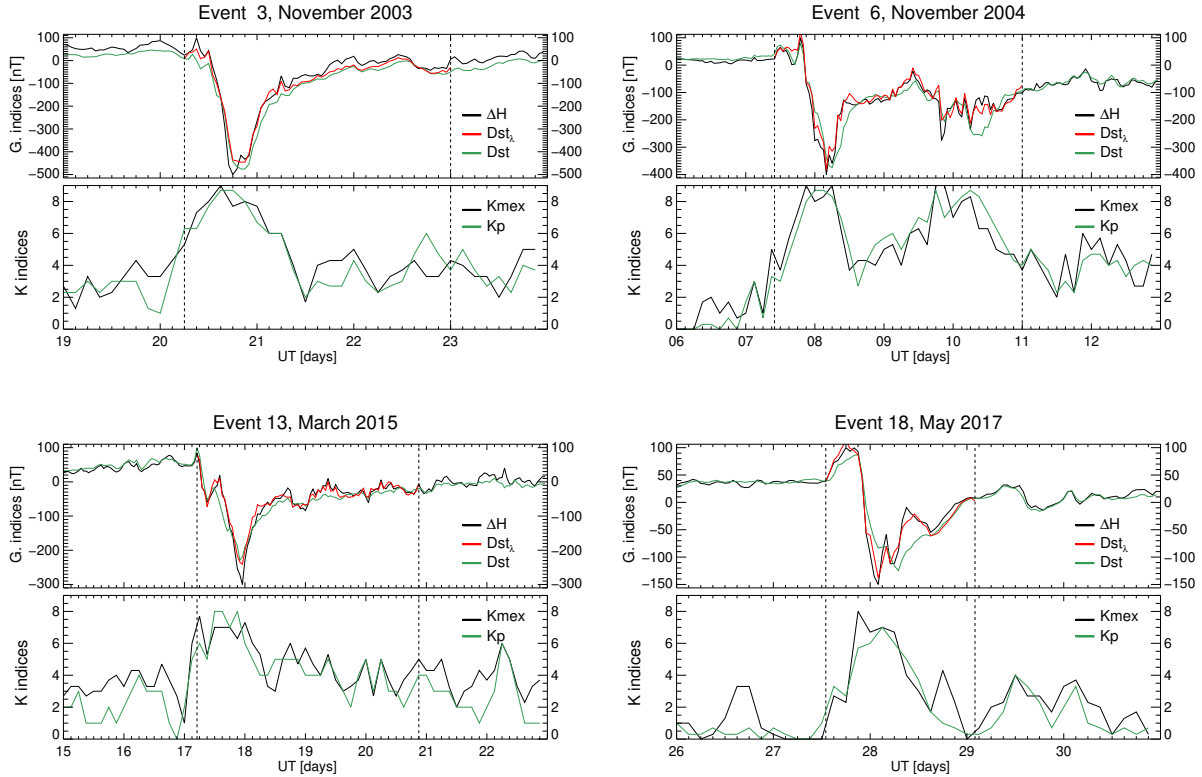


Figure 3: Comparisson between regional and planetary geomagnetic response for events 3, 6, 13 and 18. Each event shows data from Dst , ΔH , Dst_λ , K_p and K_{mex} indices. Planetary indices are depicted by green solid lines, while local geomagnetic indices are represented by black solid lines. The Dst_λ index is indicated by the red line

exercise. In all the cases, we found that Dst_λ consistently approximates ΔH . We also found that K_p with the combined effects of Dst_λ was able to enclose the regional K values.

Now, in addition to our previous qualitative comparisson; we proceed with a quantitative exploration. For this purpose we compute the average absolute difference between the pairs $\Delta H-Dst$ and $\Delta H-Dst_\lambda$ for our study cases. The results for this exploration are shown by Figure 4. In the figure we observe a histogram with the average difference between $\Delta H-Dst$ (blue bars) and $\Delta H-Dst_\lambda$ (red bars). We note that average difference associated with Dst_λ is systematically lesser than that associated with Dst . Thus the effects of magnetic perturbations consistent with those provoked by $DP2$ and $Ddyn$ are relevant for regional geomagnetic response.

Finally, our third and last step for our validation process is to remake the dispersion plot of Figure 1, but using Dst_λ data instead of Dst 's. Figure 5 shows the new dispersion plot where we can appreciate, in contrast with Figure 1, that data points (open diamonds) closely follow the identity (solid black line). Furthermore, when we compute the correlation indices we obtain note that R^2 grew from 0.77 up to 0.86 for the range of $Dst \geq -100$ nT. In addition, for the

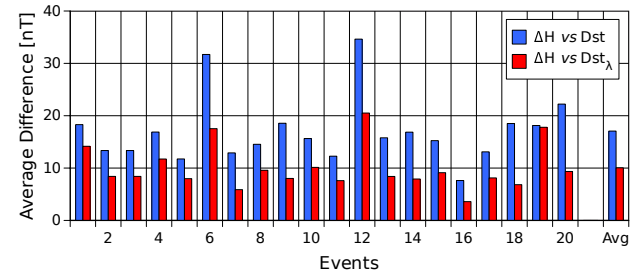


Figure 4: The average differnce between the planetary and regional geomagnetic response as registerd by Dst and ΔH indices for all the analyzed events. Blue bars represent the difference between ΔH and Dst , whereas red bars represent the difference between ΔH and Dst_λ (red bars).

case of $Dst < -100$ nT, $R^2 = 0.75$ which is significant increment from the value originally associated to Dst ($R^2 = 0.42$).

Our validation process proved that the magnetic perturbations tentatively induced by $DP2$ and $Ddyn$ ionospheric currents, when combined with planetary indices, allowed to qualitatively approximate the regional geomagnetic activity. We also proved that regional geomagnetic response, as registered by ΔH , can be quantitatively expressed by the planetary response

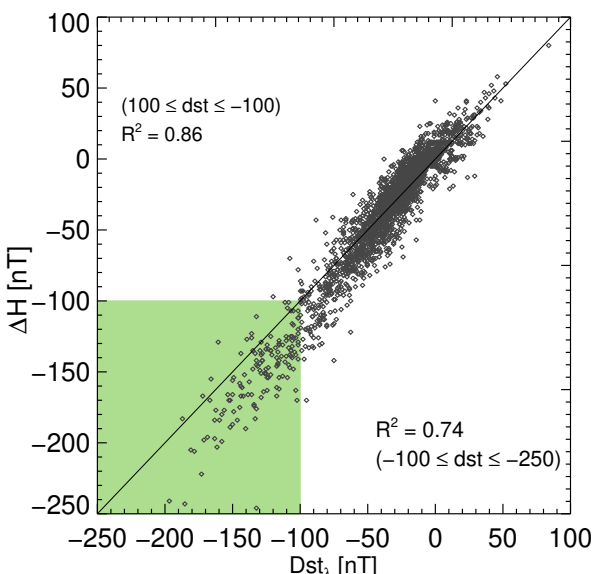


Figure 5: Dispersion plot of regional response, and planetary geomagnetic response combined with local ionospheric effects. In the vertical axis we plot ΔH and in the horizontal axis we plot Dst_λ for all analyzed events. The figure also shows the correlation indices for data with $Dst \geq -100$ nT and -250 nT $\leq Dst < -100$ nT (shadowed-green region).

(Dst) combined with the geomagnetic effects of the already commented ionospheric currents. Finally, when including the magnetic effects induced by $DP2$ and $Ddyn$ into the planetary response, the dispersion between regional and planetary data substantially decreased.

4. Concluding remarks

In this work we studied the regional manifestations of space weather at central Mexico. We focused on the differences between planetary and local geomagnetic responses during periods of strong geomagnetic storms (GS). We also investigated the possible sources for such differences in the geomagnetic response. In order to do so, we used the geomagnetic registers from the Teoloyucan Magnetic Observatory (TEO), located at north of Mexico City. We also use data sets from the Dst and K_P planetary indices, as well as the regional geomagnetic index ΔH and the total electron content delivered by the Mexican Space Weather National Laboratory (REGMEX/LANCE).

We selected 20 GS as study cases for this work (see Table 1). We identified evidence for the presence of relevant regional geomagnetic response through a dispersion plot (see Figure 1). In this regard, we found that in the range of $Dst < -100$ nT there is a tendency for the regional geomagnetic index to deviate from the planetary one. We assumed this as an evidence for regional geomagnetic response.

Subsequently, we isolated the geomagnetic effects due to ionospheric processes (D_I) from the regional (TEO) geomagnetic registers. Next, we applied filters on D_I with the purpose of identify the magnetic perturbations consistent with those induce by $Ddyn$ and $DP2$ currents. We also verified that intensification of the resulting $Ddyn$ and $DP2$ profiles simultaneously occurred during TEC perturbations (see discussion of Figure 2). In consequence, we were able to reconstruct the regional geomagnetic response consistent with those induced by $Ddyn$ and $DP2$ currents.

Afterwards, we validate our computed geomagnetic contribution due to $Ddyn$ and $DP2$ currents. First, we approximate the regional K and ΔH indices by combining the planetary K_P and Dst indices with the regional geomagnetic effects of $Ddyn$ and $DP2$. Secondly, we computed the differences between ΔH and Dst with and without the regional ionospheric effects. Finally, we analyzed the dispersion between ΔH and Dst combined with the effects of $Ddyn$ and $DP2$. For all the cases, we found that regional geomagnetic response is qualitatively and quantitatively approximated by the geomagnetic planetary response combined with the geomagnetic perturbations induced by the $Ddyn$ and $DP2$ ionospheric currents.

Thus, our study shows that regional space-weather manifestations at central Mexico may significantly deviate from the planetary response. In consequence, in order to address the regional effects of, and risks due to, space-weather in Central Mexico, it is necessary to carry out studies from a regional approach, complemented with the planetary context. Our results highlight the particularities that geomagnetic response has for a given location. Hence, in order to achieve a better understanding of space weather and to improve the operational response, our results evidence for the necessity to include more registers (magnetometers) into the computing of geomagnetic indices, whether planetary or regional.

Hence, according to our results, during intense geomagnetic storms, in central Mexico, the effects of $Ddyn$ and $DP2$ may induce alterations in the F region of the ionosphere and displace the equatorial ionospheric anomaly towards central and southern regions of Mexico (as showed by Sergeeva et al., 2020). Therefore we could expect these phenomena lead to ionospheric scintillation, which degrades satellite communications, as well as the precision of navigation and positioning systems, among other services. All these effects can potentially be addressed through local perturbations of the TEC during geomagnetic storm periods (refer to panels (e) of Figure 2).

It is important to remark that the surface of Mexico is near 2 million km². This fact made of our results valid only for the central region of Mexico (few thousands of km²), leaving the rest of its surface to address. In addition, Mexico is located at North America, and

the ionospheric currents pass through and evolve along the whole American continent. Hence, on one hand, it is required more sources of geomagnetic registers in Mexico and, on the other hand, it is necessary to contextualize the geomagnetic response of Mexico with those present in Northern and Central America, and even South America. For the first case, LANCE is developing a the Network of Geomagnetic Stations Mexico (REGMEX) (see Corona-Romero et al., 2024), to monitoring regional geomagnetic response all over Mexico. Whereas, for the case of contextualize the geomagnetic response of Mexico, this is our immediate future work.

CRediT authorship contribution statement

Castellanos-Velazco, C. I.: Methodology, Conceptualization, Data analysis, Software, Data processing, Writing - Original Draft. **Corona-Romero, P.:** Conceptualization, Methodology, Regional indices computation, Writing - Review & Editing. **González-Esparza, J. A.:** Data revision, Review & Editing. **Sergeeva, M. A.:** Local ionospheric data, Review & Editing. **Caccavari-Garza, A. L.:** Regional magnetic data. **Gatica-Acevedo, V. J.:** Local ionospheric data, Ionospheric data processing.

Declaration of competing interest

The authors declare that they have no known competing financial interests or personal relationships that could have appeared to influence the work reported in this paper.

Data Availability

Data will be made available on request.

Acknowledgments

P. Corona-Romero is grateful for Investigadores por Mexico-CONAHCYT (CONAHCYT Research Fellow) project 1045 Space Weather Service, financed by “Consejo Nacional de Ciencia y Tecnología” (CONAHCYT), which partially supported this work. C.I. Castellanos-Velazco is grateful for “La Beca de Posgrado en Mexico” granted by CONAHCYT. LANCE acknowledges partial financial support from CONHACyT-AEM grant 2017-01-292684, CONAHCyT LN-315829, and PAPIIT IN116023.

This work used data from the Teoloyucan Magnetic Observatory operated by the Magnetic Service of the Geophysics Institute at National and Autonomous University of Mexico (UNAM). Total electron content (*TEC*) and the geomagnetic indices ΔH and K , the regional counterparts of *Dst* and K_P indices respectively, are produced by the Geomagnetic Stations Network of

Mexico (REGMEX) by the Mexican Space Weather National Laboratory (LANCE), Geophysics Institute at National and Autonomous University of Mexico (UNAM).

The results presented in this paper rely on K_P and *Dst* geomagnetic indices calculated by the Helmholtz-Zentrum Potsdam Deutsches GeoForschungsZentrum Adolf-Schmidt-Observatorium and the World Data Center for Geomagnetism, Kyoto, respectively, from data collected at magnetic observatories. We thank the involved national institutes, the INTERMAGNET network and ISGI.

All authors have seen and approved the final version of the manuscript.

References

- Akala, A.O., Oyeyemi, E.O., Amaechi, P.O., Radicella, S.M., Nava, B., Amory-Mazaudier, C., 2020. Longitudinal Responses of the Equatorial/Low-Latitude Ionosphere Over the Oceanic Regions to Geomagnetic Storms of May and September 2017. *Journal of Geophysical Research (Space Physics)* 125, e27963. doi:10.1029/2020JA027963.
- Amory-Mazaudier, C., Bolaji, O.S., Doumbia, V., 2017. On the historical origins of the CEJ, DP2, and Ddyn current systems and their roles in the predictions of ionospheric responses to geomagnetic storms at equatorial latitudes. *Journal of Geophysical Research (Space Physics)* 122, 7827–7833. doi:10.1002/2017JA024132.
- Bailey, R.L., Halbedl, T.S., Schattauer, I., Römer, A., Achleitner, G., Beggan, C.D., Wesztergom, V., Egli, R., Leonhardt, R., 2017. Modelling geomagnetically induced currents in midlatitude Central Europe using a thin-sheet approach. *Annales Geophysicae* 35, 751–761. doi:10.5194/angeo-35-751-2017.
- Baumjohann, W., Treumann, R.A., 1999. Basic Space Plasma Physics. Imperial College Press, 57 Shelton Street Covent Garden London WC2H 9HE.
- Blanc, M., Caudal, G., 1985. The spatial distribution of magnetospheric convection electric fieldsat ionospheric altitudes: a review. II. Theories. *Annales Geophysicae* 3, 27–42.
- Blanc, M., Richmond, A.D., 1980. The ionospheric disturbance dynamo. *Journal of Geophysical Research* 85, 1669–1686. doi:10.1029/JA085iA04p01669.
- Bobova, V.P., Vladimirkii, B.M., Pudovkin, M.I., 1985. The presence in the AE index of 160-minute pulsations evidently caused by solar pulsations. *Izvestiya Ordena Trudovogo Krasnogo Znameni Krymskoj Astrofizicheskoy Observatorii* 71, 19–25.
- Carrillo-Vargas, A., Pérez-Enríquez, R., Rodríguez-Martínez, M., López-Montes, R., Casillas-Pérez, G.A., Araujo-Pradere, E.A., 2012. Ionospheric disturbances detected by MEXART. *Advances in Space Research* 49, 1570–1580. doi:10.1016/j.asr.2011.12.017.
- Corona-Romero, P., Gonzalez-Esparza, J., Villanueva-Hernandez, P., Andrade-Mascote, E., Castellanos-Velazco, C., Espinosa-Jimenez, A., Sergeeva, M., 2024. The geomagnetic stations network of mexico (regmex): The initial steps towards a real-time monitoring of geomagnetic activity in mexico. *Journal of Atmospheric and Solar-Terrestrial Physics* 256, 106204. URL: <https://www.sciencedirect.com/science/article/pii/S1364682624000324>, doi:<https://doi.org/10.1016/j.jastp.2024.106204>.
- Corona-Romero, P., Sanchez-Garcia, E., Sergeeva, M., Gonzalez-Esparza, J., Cifuentes-Nava, G., Hernandez-Quintero, E., Caccavari, A., Aguilar-Rodriguez, E., Mejía-Ambriz, J., de-la-Luz, V., Gonzalez, L., 2018. Kmex: the mexican geomagnetic k

- index, in: Proceedings of the II Pan-American Workshop on Geomagnetism, Basouras, Brazil. pp. 96–100.
- Corona-Romero, P., Sergeeva, M., Gonzalez-Esparza, J., Cifuentes-Nava, G., Hernandez-Quintero, E., Caccavari, A., Sanchez-Garcia, E., 2017. Mexican geomagnetic k index , 1–6.
- C.T Russell, J. G. Luhman, R.J.S., 2016. SPACE PHYSICS AN INTRODUCTION. Cambridge university press. University Princting House, Cambridge CB2 (BS, United Kingdom.
- da Silva Barbosa, C., Hartmann, G.A., Pinheiro, K.J., 2015. Numerical modeling of geomagnetically induced currents in a Brazilian transmission line. *Advances in Space Research* 55, 1168–1179. doi:10.1016/j.asr.2014.11.008.
- Denisenko, V.V., Zamai, S.S., Kitaev, A.V., Matveenkov, I.T., Pivovarov, V.G., 1992. System of ionospheric currents excited by a magnetospheric generator in the boundary layer. *Geomagnetism and Aeronomy* 32, 142–145.
- Gjerloev, J.W., 2012. The SuperMAG data processing technique. *Journal of Geophysical Research (Space Physics)* 117, A09213. doi:10.1029/2012JA017683.
- Gonzalez, W.D., Joselyn, J.A., Kamide, Y., Kroehl, H.W., Rostoker, G., Tsurutani, B.T., Vasyliunas, V.M., 1994. What is a geomagnetic storm? *Journal of Geophysical Research* 99, 5771–5792. doi:10.1029/93JA02867.
- Gonzalez-Esparza, A., Carrillo, A., Andrade, E., Jeyakumar, S., Ananthakrishnan, S., Praveenkumar, A., Sankarasubramanian, G., Sureshkumar, S., Sierra, P., Vazquez, S., Perez-Enriquez, R., Kurtz, S., 2005. MEXART Measurements of Radio Sources. Interplanetary Scintillation Array in Mexico, in: AGU Fall Meeting Abstracts, pp. SH51C–1218.
- Gonzalez-Esparza, J.A., De la Luz, V., Corona-Romero, P., Mejia-Ambriz, J.C., Gonzalez, L.X., Sergeeva, M.A., Romero-Hernandez, E., Aguilar-Rodriguez, E., 2017. Mexican space weather service (sciesmex). *Space Weather* 15, 3–11. URL: <https://agupubs.onlinelibrary.wiley.com/doi/abs/10.1002/2016SW001496>. doi:<https://doi.org/10.1002/2016SW001496>.
- Hejda, P., Bochníček, J., 2005. Geomagnetically induced pipe-to-soil voltages in the Czech oil pipelines during October–November 2003. *Annales Geophysicae* 23, 3089–3093. doi:10.5194/angeo-23-3089-2005.
- Heppner, J.P., 1972a. Electric Fields in the Magnetosphere, in: Dyer, E.R. (Ed.), Critical Problems of Magnetospheric Physics, p. 107.
- Heppner, J.P., 1972b. Polar-cap electric field distributions related to the interplanetary magnetic field direction. *Journal of Geophysical Research* 77, 4877–4887. doi:10.1029/JA077i025p04877.
- Kikuchi, T., Hashimoto, K.K., 2016. Transmission of the electric fields to the low latitude ionosphere in the magnetosphere-ionosphere current circuit. *Geoscience Letters* 3, 4. doi:10.1186/s40562-016-0035-6.
- Knecht, D., B.M., .S., 1985. HANDBOOK OF GEOPHYSICS AND THE SPACE ENVIRONMENT, chapter 4, THE GEOMAGNETIC FIELD. ed by A. S. Jursa, Boston: Air Force Geophysics Laboratory.
- Le Huy, M., Amory-Mazaudier, C., 2005. Magnetic signature of the ionospheric disturbance dynamo at equatorial latitudes: “ D_{dyn} ”. *Journal of Geophysical Research (Space Physics)* 110, A10301. doi:10.1029/2004JA010578.
- López-Montes, R., Pérez-Enríquez, R., Araujo-Pradere, E.A., 2012. The impact of large solar events on the total electron content of the ionosphere at mid latitudes. *Advances in Space Research* 49, 1167–1179. doi:10.1016/j.asr.2012.01.008.
- Martínez-Bretón L., J., Ortega, B.M., Hernandez-Quintero, J.E., 2016. Relationship between the minima of the horizontal magnetic component measured in mexico and the dst and symh indices for geomagnetic storms with dst -100nt during the descending phase of solar cycle 23. *Geofísica Internacional* 55, 155–164.
- Mayaud, P.N., 1980. Derivation, Meaning, and Use of Geomagnetic Indices. *Geophysical Monograph Series* 22, 607. doi:10.1029/GM022.
- Merline Matamba, T., Habarulema, J.B., Burešová, D., 2016. Midlatitude ionospheric changes to four great geomagnetic storms of solar cycle 23 in Southern and Northern Hemispheres. *Space Weather* 14, 1155–1171. doi:10.1002/2016SW001516.
- Nishida, A., 1966. Formation of plasmapause, or magnetospheric plasma knee, by the combined action of magnetospheric convection and plasma escape from the tail. *Journal of Geophysical Research* 71, 5669–5679. doi:10.1029/JZ071i023p05669.
- Nishida, A., 1968a. Coherence of geomagnetic DP 2 fluctuations with interplanetary magnetic variations. *Journal of Geophysical Research* 73, 5549–5559. doi:10.1029/JA073i017p05549.
- Nishida, A., 1968b. Geomagnetic D_p 2 fluctuations and associated magnetospheric phenomena. *Journal of Geophysical Research* 73, 1795–1803. doi:10.1029/JA073i005p01795.
- Obayashi, T., Nishida, A., 1968. Large-Scale Electric Field in the Magnetosphere. *Space Science Reviews* 8, 3–31. doi:10.1007/BF00362569.
- Pérez-Enríquez, R., Kotsarenko, A., 2003. IPS data of the Mexican Array Radio Telescope (MEXART) corrected for ionospheric scintillation and geomagnetic activity, in: EGS - AGU - EUG Joint Assembly, p. 2923.
- Pirjola, R., 2000. Geomagnetically induced currents during magnetic storms. *IEEE Transactions on Plasma Science* 28, 1867–1873. doi:10.1109/27.902215.
- Rishbeth, H., Garriott, O.K., 1969. Introduction to ionospheric physics.
- Rodriguez-Martinez, M., Perez-Enriquez, R., Carrillo-Vargas, A., Lopez-Montes, R., Araujo-Pradere, E.A., Casillas-Perez, G., Lopez Cruz-Abeyro, J., 2011. Ionospheric Disturbance Effects on IPS signals from MEXART, in: AGU Fall Meeting Abstracts, pp. SH13B–1969.
- Rodriguez-Martinez, M., Perez-Enriquez, R., Carrillo-Vargas, A., López-Montes, R., Araujo-Pradere, E., Casillas, G., Lopez Cruz-Abeyro, J., 2011. Ionospheric disturbance effects on ips signals from mexart. AGU Fall Meeting Abstracts , 1969–.
- Rodriguez-Martinez, M., Pérez-Enríquez, H., Carrillo-Vargas, A., López-Montes, R., Araujo-Pradere, E., Casillas, G., Lopez Cruz-Abeyro, J., 2014. Ionospheric disturbances and their impact on ips using mexart observations. *Solar Physics* 289. doi:10.1007/s11207-014-0496-8.
- Romero-Hernandez, E., Gonzalez-Esparza, J.A., Rodriguez-Martinez, M., Sergeeva, M.A., Aguilar-Rodriguez, E., Mejia-Ambriz, J.C., De la Luz, V., 2017. Study of ionospheric disturbances over Mexico associated with transient space weather events. *Advances in Space Research* 60, 1838–1849. doi:10.1016/j.asr.2017.06.042.
- Schrijver, C.J., 2015. Socio-Economic Hazards and Impacts of Space Weather: The Important Range Between Mild and Extreme. *Space Weather* 13, 524–528. doi:10.1002/2015SW001252, arXiv:1507.08730.
- Sergeeva, M., Kalishin, A., Maltseva, O., Blagoveshchensky, D., Gonzalez-Esparza, A., Corona-Romero, P., Gatica Acevedo, V., 2020. Possibility of signal reflection from the northern crest of eia: case study , 1–4doi:10.23919/EuCAP48036.2020.9135786.
- Sergeeva, M.A., Gonzalez-Esparza, J.A., Blagoveshchensky, D.V., Maltseva, O.A., Chernov, A.G., Corona-Romero, P., De la Luz, V., Mejia-Ambriz, J.C., Gonzalez, L.X., Romero-Hernandez, E., Rodriguez-Martinez, M., Aguilar-Rodriguez, E., Andrade, E., Villanueva, P., Gatica-Acevedo, V.J., 2019. First observations of oblique ionospheric sounding chirp signal in Mexico. *Results in Physics* 12, 1002–1003. doi:10.1016/j.

- rinp.2018.12.077.
- Sergeeva, M.A., Maltseva, O.A., Gonzalez-Esparza, J.A., De la Luz, V., Corona-Romero, P., 2017. Features of TEC behaviour over the low-latitude North-American region during the period of medium solar activity. *Advances in Space Research* 60, 1594–1605. doi:10.1016/j.asr.2017.06.021.
- van de Kamp, M., 2013. Harmonic quiet-day curves as magnetometer baselines for ionospheric current analyses. *Geoscientific Instrumentation, Methods and Data Systems* 2, 289–304. doi:10.5194/gi-2-289-2013.
- Vankadara, R.K., Panda, S.K., Amory-Mazaudier, C., Fleury, R., Devananboyina, V.R., Pant, T.K., Jamjareegulgarn, P., Haq, M.A., Okoh, D., Seemala, G.K., 2022. Signatures of Equatorial Plasma Bubbles and Ionospheric Scintillations from Magnetometer and GNSS Observations in the Indian Longitudes during the Space Weather Events of Early September 2017. *Remote Sensing* 14, 652. doi:10.3390/rs14030652.
- Vodyannikov, V.V., Gordienko, G.I., Nechaev, S.A., Sokolova, O.I., Khomutov, S.Y., Yakovets, A.F., 2006. Geomagnetically induced currents in power lines according to data on geomagnetic variations. *Geomagnetism and Aeronomy* 46, 809–813. doi:10.1134/S0016793206060168.
- Wei, Y., Zhao, B., Li, G., Wan, W., 2015. Electric field penetration into Earth's ionosphere: a brief review for 2000–2013. *Science Bulletin* 60, 748–761. doi:10.1007/s11434-015-0749-4.
- Yamazaki, Y., Häusler, K., Wild, J.A., 2016. Day-to-day variability of midlatitude ionospheric currents due to magnetospheric and lower atmospheric forcing. *Journal of Geophysical Research (Space Physics)* 121, 7067–7086. doi:10.1002/2016JA022817.
- Younas, W., Amory-Mazaudier, C., Khan, M., Fleury, R., 2020. Ionospheric and Magnetic Signatures of a Space Weather Event on 25–29 August 2018: CME and HSSWs. *Journal of Geophysical Research (Space Physics)* 125, e27981. doi:10.1029/2020JA027981.
- Zaka, K.Z., Kobeia, A.T., Assamoi, P., Obrou, O.K., Doumbia, V., Boka, K., Adohi, B.J.P., Mene, N.M., 2009. Latitudinal profile of the ionospheric disturbance dynamo magnetic signature: comparison with the DP2 magnetic disturbance. *Annales Geophysicae* 27, 3523–3536. doi:10.5194/angeo-27-3523-2009.

A. Analysis and Results

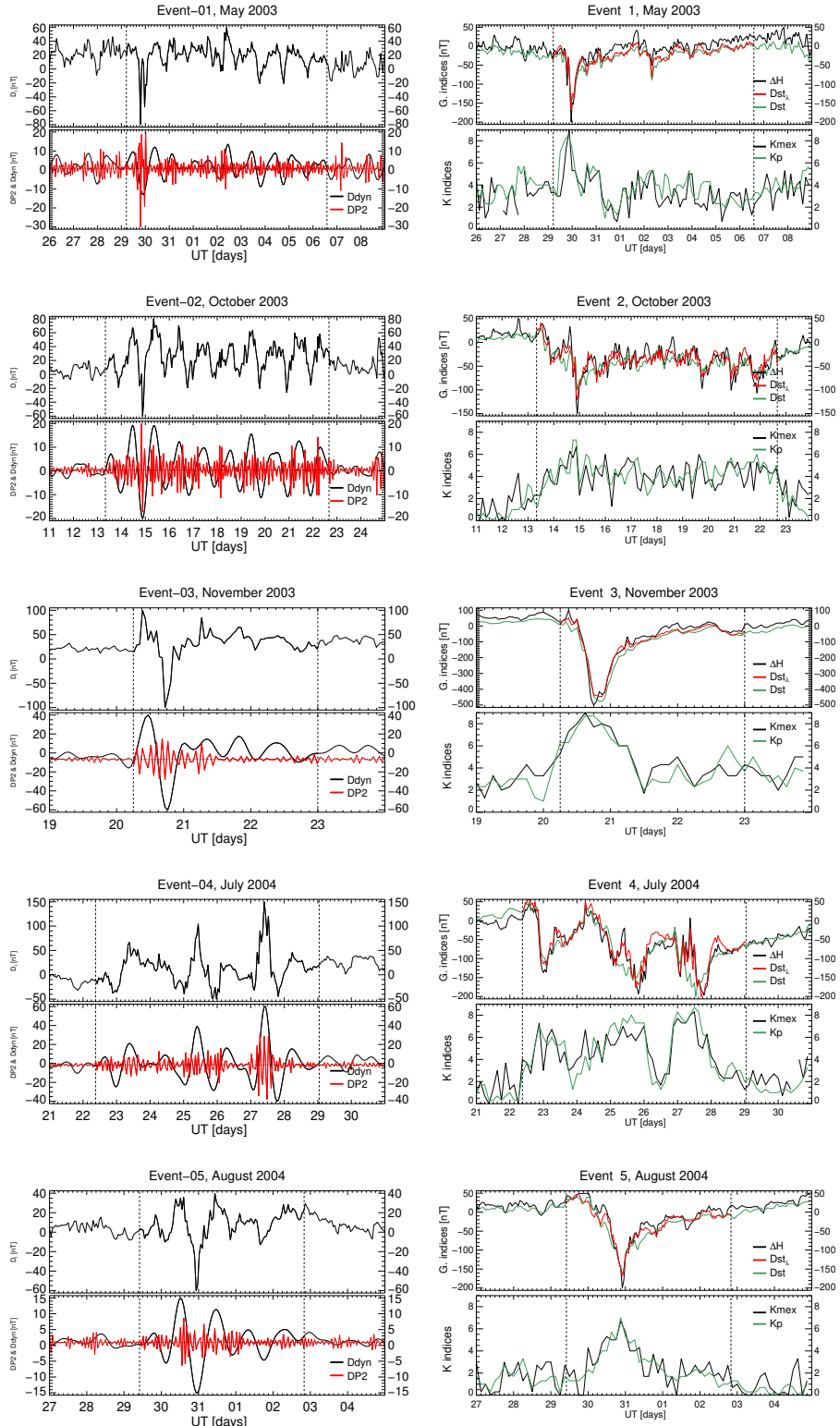


Figure 6: On the right side, top panels illustrate the contribution of Ionospheric Magnetic Disturbances, while bottom panels depict the isolated geomagnetic contributions of D_{dyn} and DP_2 . The vertical dashed lines highlight the geomagnetic storm time period during which such calculations are valid. On the left side, green lines represent planetary indices, while black lines denote local indices. Additionally, red lines represent the approximation of ΔH at top, while bottom showcases the comparison of local K (black line) and planetary K (green line).

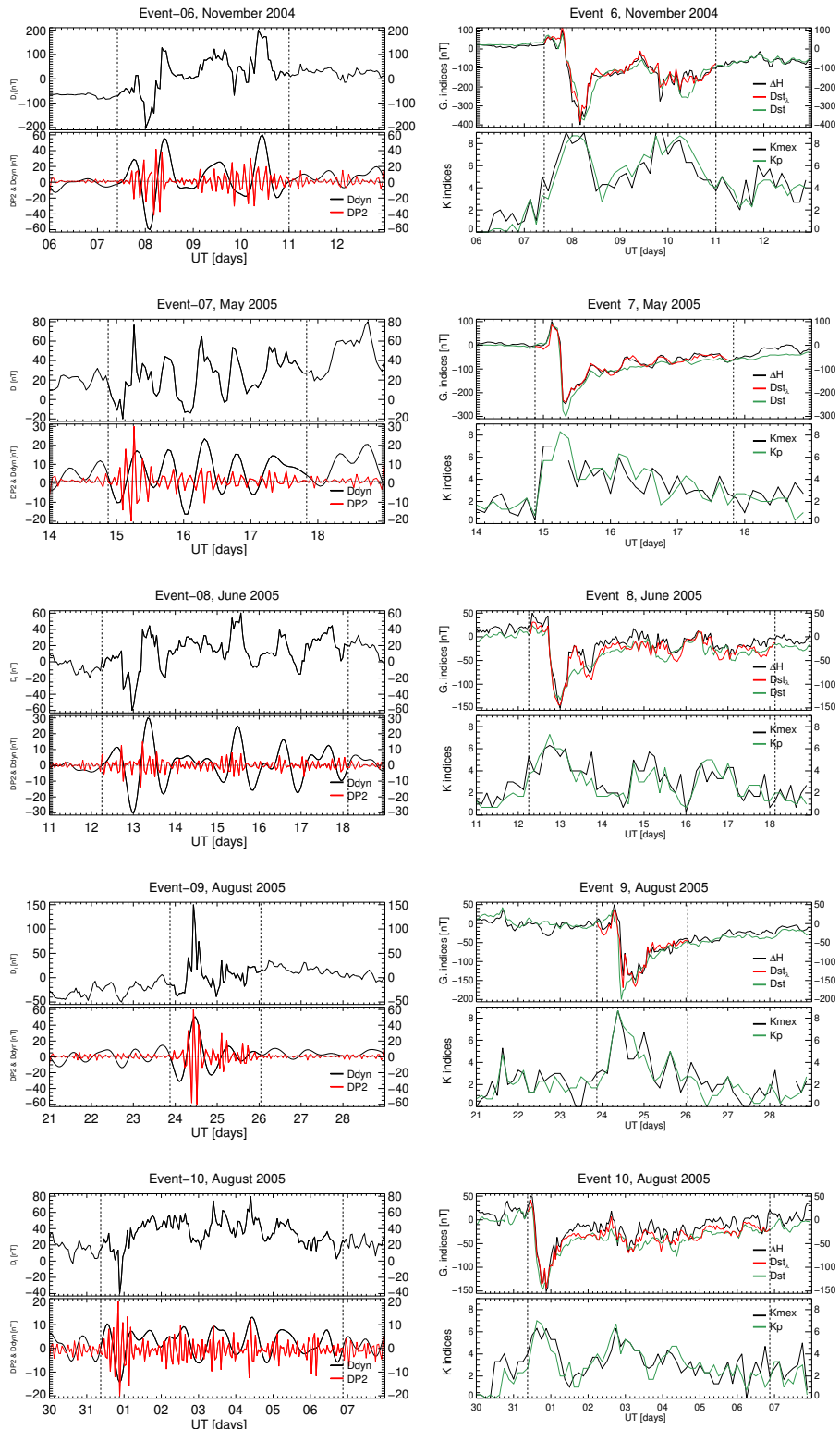


Figure 7: On the right side, top panels illustrate the contribution of Ionospheric Magnetic Disturbances, while bottom panels depict the isolated geomagnetic contributions of D_{dyn} and $DP2$. The vertical dashed lines highlight the geomagnetic storm time period during which such calculations are valid. On the left side, green lines represent planetary indices, while black lines denote local indices. Additionally, red lines represent the approximation of ΔH at top, while bottom showcases the comparison of local K (black line) and planetary K (green line).

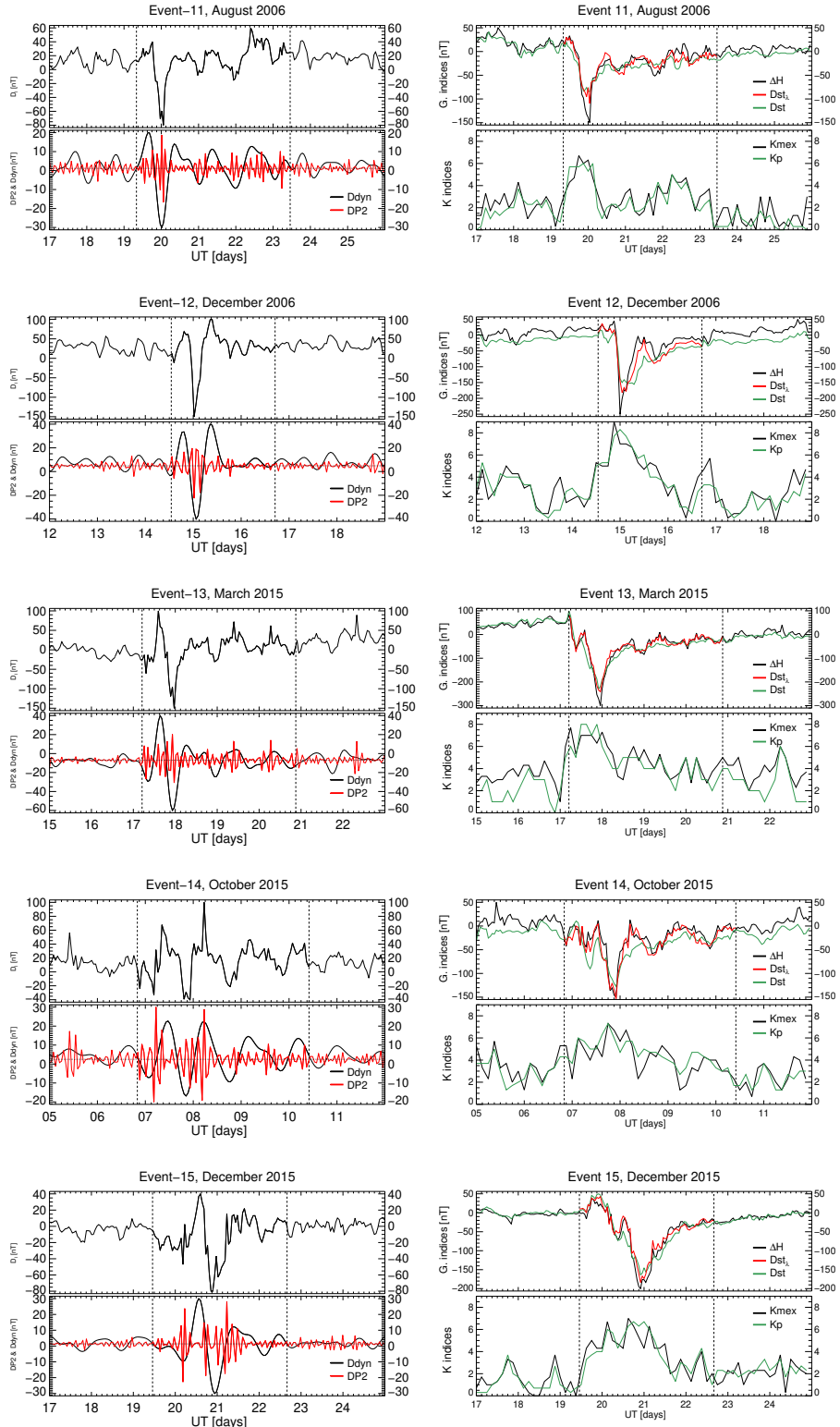


Figure 8: On the right side, top panels illustrate the contribution of Ionospheric Magnetic Disturbances, while bottom panels depict the isolated geomagnetic contributions of D_{dyn} and DP_2 . The vertical dashed lines highlight the geomagnetic storm time period during which such calculations are valid. On the left side, green lines represent planetary indices, while black lines denote local indices. Additionally, red lines represent the approximation of ΔH at top, while bottom showcases the comparison of local K (black line) and planetary K (green line).

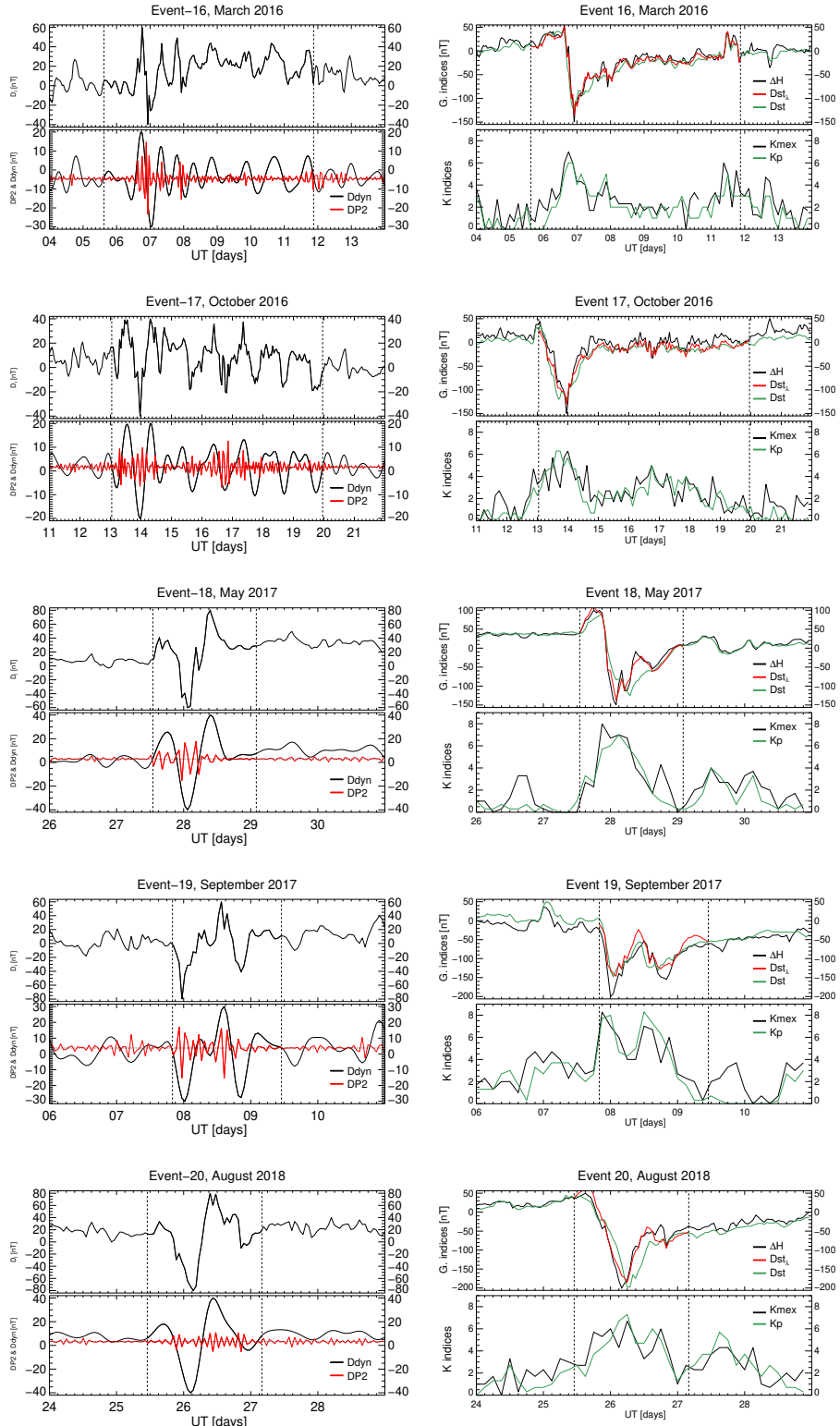


Figure 9: On the right side, top panels illustrate the contribution of Ionospheric Magnetic Disturbances, while bottom panels depict the isolated geomagnetic contributions of $Ddyn$ and $DP2$. The vertical dashed lines highlight the geomagnetic storm time period during which such calculations are valid. On the left side, green lines represent planetary indices, while black lines denote local indices. Additionally, red lines represent the approximation of ΔH at top, while bottom showcases the comparison of local K (black line) and planetary K (green line).